DOI: https://doi.org/10.68732/54c29f1da2e919a5

ISBN: 978-9989-2053-7-8

Impact of elastic and strength anisotropy on seal integrity in energy storage

Daniel Bücken
Ruhr University Bochum, Bochum, Germany
Geomecon GmbH, Berlin, Germany
daniel.buecken@rub.de
0009-0007-8575-8740

Tobias Backers
Ruhr University Bochum, Bochum, Germany

Ki-Bok Min
Seoul National University, Seoul, Republic of Korea

Subsurface thermo-mechanical energy storage approaches such as supercharged hybrid gas-based energy storage (SH-GES) lead to significant poro- and thermoelastic stress changes, possibly affecting the integrity of the sealing formations. In clastic reservoir systems, these formations typically consist of shales or similar lithologies, often characterised by bedding parallel transversely isotropic material behaviour. In this study, the effect of both elastic and strength anisotropy of the sealing formation is assessed by means of coupled multiphase thermo-hydro-mechanical simulations. An anisotropy ratio of E/E' = 1.66 was used for the transversely isotropic sealing formation. The results are compared to the behaviour of an isotropic reference case. Two reservoir permeabilities were considered. Strength anisotropy is implemented using the single plane of weakness approach, with implicit weakness planes characterised by a lower friction coefficient (μ_{weak} = 0.37) and lower cohesion ($c_{0,weak}$ = 9.6 MPa) than the intact rock. The effect of weakness plane orientation is assessed by a systematic variation of dip angle and azimuth. The results show that the elastic anisotropy made only minor differences in seal integrity between isotropic and transversely isotropic cases, regardless of reservoir permeability. Instead, seal integrity is predominantly controlled by weakness plane orientation and reservoir permeability. The analysis of Coulomb Failure Stress (CFS) shows that during energy storage operations, i.e., cyclic injection of CO_2 and production, seal stability changes significantly even when the seal was stable initially. This is attributed to dynamic stress rotations induced by thermo-poro-elastic effects. These findings highlight the necessity of time-dependent numerical analyses to accurately assess seal integrity in thermo-mechanical gas-based energy storage systems and other geo-energy applications.

Keywords

Energy storage, Transverse isotropy, Strength anisotropy, SH-GES.

1 Introduction

Increasing the share of green energies such as wind and solar energy requires dependable energy storage solutions (Gallo et al., 2016; Wang et al., 2022). Geological storage solutions

are promising (Buursink et al., 2023), but require a solid understanding of the geomechanical behaviour (Paluszny & Zimmerman, 2025). Subsurface thermo-mechanical energy storage approaches such as supercharged hybrid gas-based energy storage (SH-GES; Bücken & Backers, 2023) using CO_2 as a working fluid are energetically advantageous (Li et al., 2023), do however lead to significant poro- and thermoelastic stress changes, possibly affecting the integrity of the sealing formations (Bücken et al., 2026; Bücken & Backers, 2025). In clastic reservoir systems, these formations typically consist of shales or similar lithologies, often characterised by bedding parallel transversely isotropic material behaviour (Winkler et al., 2023). This study investigates how strength anisotropy (modelled using implicit weakness planes) and elastic anisotropy (represented by transversely isotropic parameters) affect the geomechanical integrity of the sealing formation in an SH-GES system through coupled thermo-hydro-mechanical (THM) simulations.

2 Methodology

The numerical simulations are carried out in COMSOL Multiphysics®. A generic subsurface geometry is assumed (Fig. 1). The reservoir and seal formations are horizontal and50 m thick each. A single borehole is placed in the centre of the reservoir, with an open-hole length of 40 m. The reservoir top is at 2,475 m depth.

Transient thermo-poroelastic effects in the reservoir and the adjacent sealing formation, caused by cyclic loading and unloading of the reservoir, are modelled using linear elasticity. An external stress field typical for Central Europe is applied (gradient vertical stress SV = 25 MPa/km, gradient maximum horizontal stress SH = 25.5 MPa/km, gradient minimum horizontal stress Sh = 18 MPa/km), with the direction of SH aziSH = 000° (N-S). Multiphase flow of CO_2 and water is explicitly modelled. The model is initially water filled with hydrostatic pore pressure and a geothermal gradient of 30 K/km with a ground-level temperature of 10 °C. Chemical effects are not accounted for in this study.

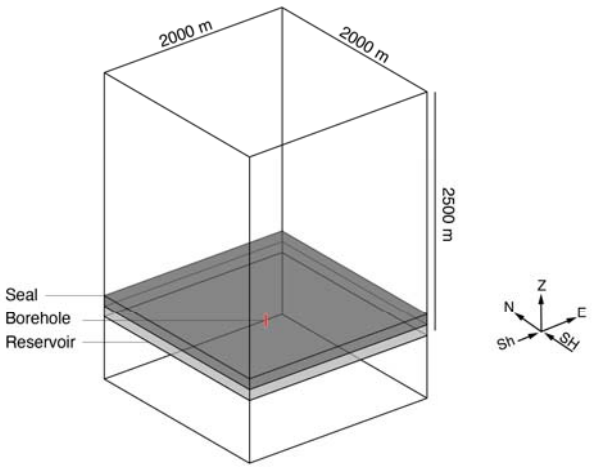


Fig. 1 Subsurface model. The red borehole interval represents the open-hole section.

In total, 6.5 years of storage operations are modelled. Firstly, constant injection of CO_2 is modelled over 1.5 years to condition the reservoir. Then, 5 years of cyclic operations, consisting of 40-day pumping phases alternating with 15-day pauses, are modelled. A pump rate of 25 kg/s and a temperature difference of + 50 K relative to the in-situ temperature are used.

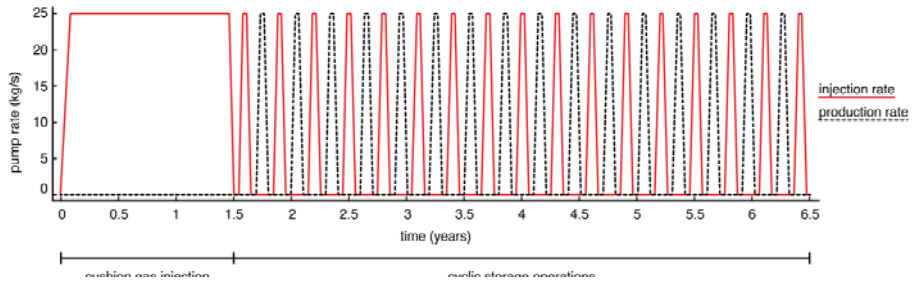


Fig. 2 Injection and production scheme of the simulated SH-GES operations.

The petrophysical parameters of the reservoir and seal formation are detailed in Table 1. The reservoir parameters are based on typical values for clastic reservoirs as well as laboratory measurements (Neumann et al., 2025). The mechanical parameters of the seal are based on the German Posidonia shale (Meier, 2017), resulting in an anisotropy ratio of E/E' = 1.66 for the transversely isotropic sealing formation. Two reservoir permeabilities are considered to capture the impact of reservoir permeability.

The results of the transversely isotropic seal are compared to the behaviour of an isotropic reference case. Seal integrity is evaluated using the single plane of weakness approach (Hudson et al., 2002; Jaeger, 1960; McLamore & Gray, 1967) as well as Coulomb Failure Stress (CFS = τ - $\mu \cdot \sigma_n$ - C_o; τ: shear stress, μ: friction coefficient, σ_n: normal stress, C_o: cohesion), with implicit weakness planes characterised by a lower friction coefficient and lower cohesion than the intact rock. The effect of weakness plane orientation is assessed by a systematic variation of dip angle and dip direction. Plane orientations are denoted as (dip direction)/(dip angle), both in degrees. The weakness planes are modelled implicitly, hence not affecting the stresses in the system.

Table 1. Petrophysical model parameters. ISO: isotropic scenario; TI: transversely isotropic scenario; WP: weakness plane.

Parameter		Unit	Reservoir	Seal	
Young's modulus (ISO)	E	[GPa]	20	17.3	
Poisson's ratio (ISO)	ν	[1]	0.25	0.18	
Young's modulus (TI)	E	[GPa]	20	E: 10.4	E': 17.3
Poisson's ratio (TI)	ν	[1]	0.25	ν: 0.3	ν': 0.18
Shear modulus (TI)	G	[GPa]	—	G': 5.5	
Friction coefficient	μ	[1]	0.85	μ_{intact}: 0.48	μ_{WP}: 0.37
Cohesion	C_o	[MPa]	—	$C_{o,intact}$: 22.3	$C_{o,WP}$: 9.6
Density	ρ	[kg/m^3]	2,500	2,500	
Biot coefficient	α_B	[1]	1	1	
Porosity	Φ	[1]	0.2	0.01	
Permeability	k	[mD]	50 – 1,000	1E-4	
Coefficient of thermal expansion	α_T	[1/K]	12E-6	6E-6	
Specific heat capacity	C	[J/(kg·K)]	850	850	
Thermal conductivity	k_T	[W/(m·K)]	3	3	

3 Results and discussion

While destabilised relative to the initial conditions, the seal remains stable in all modelled scenarios (i.e., CFS < 0; Fig. 3). Initial seal stability is controlled by the orientation of the weakness planes relative to the in-situ stress field. The relative orientation is quantified by the angle θ, defined as the angle between the maximum principal in-situ stress σ_1 and the normal

to the weakness plane. The highest initial CFS values are reached for θ_{ini} = 60° – 65° (initial θ angles). The least stable orientations are hence 000/30, 030/30, 060/60, and 060/90. This is consistent with the single plane of weakness approach, which defines the most critical value of θ as $\theta_{crit} = 45° + \phi_{WP}/2$ where ϕ_{WP} is the friction angle of the weakness plane. For $\phi_{WP} = \arctan(\mu_{WP})$, the most critical weakness plane orientation is reached for θ_{crit} = 55°. The temporal evolution of the maximum CFS value per timestep (Fig. 3) however reveals that the initial CFS does not predict the largest CFS value reached during SH-GES operations.

The greatest destabilisation, i.e. the largest increase in CFS (ΔCFS > 0) occurs in the initially most stable scenario (000/90, Fig. 3). This indicates that initial stress conditions are not necessarily indicative of the time-dependent geomechanical performance. In all cases the maximum CFS is reached shortly after the beginning of the initial injection. This is consistent with previous studies, highlighting the strong influence of thermo-elastic stress redistributions (Bücken et al., 2026). Except for the 090/90 scenario, which remains the most stable overall, all scenarios reach nearly identical maximum CFS values.

For both reservoir permeabilities, the influence of the transversely isotropic elastic properties on seal stability is minor only. The transversely isotropic cases tend to be slightly more critical, but this trend is neither systematic nor dominant (Fig. 3). This is attributed to the comparatively low anisotropy ratio of E/E' = 1.66. In contrast, reservoir permeability has a more pronounced effect on seal stability. Consistent with previous studies, a lower reservoir permeability leads to higher CFS values in the seal (Bücken et al., 2026; Bücken & Backers, 2025).

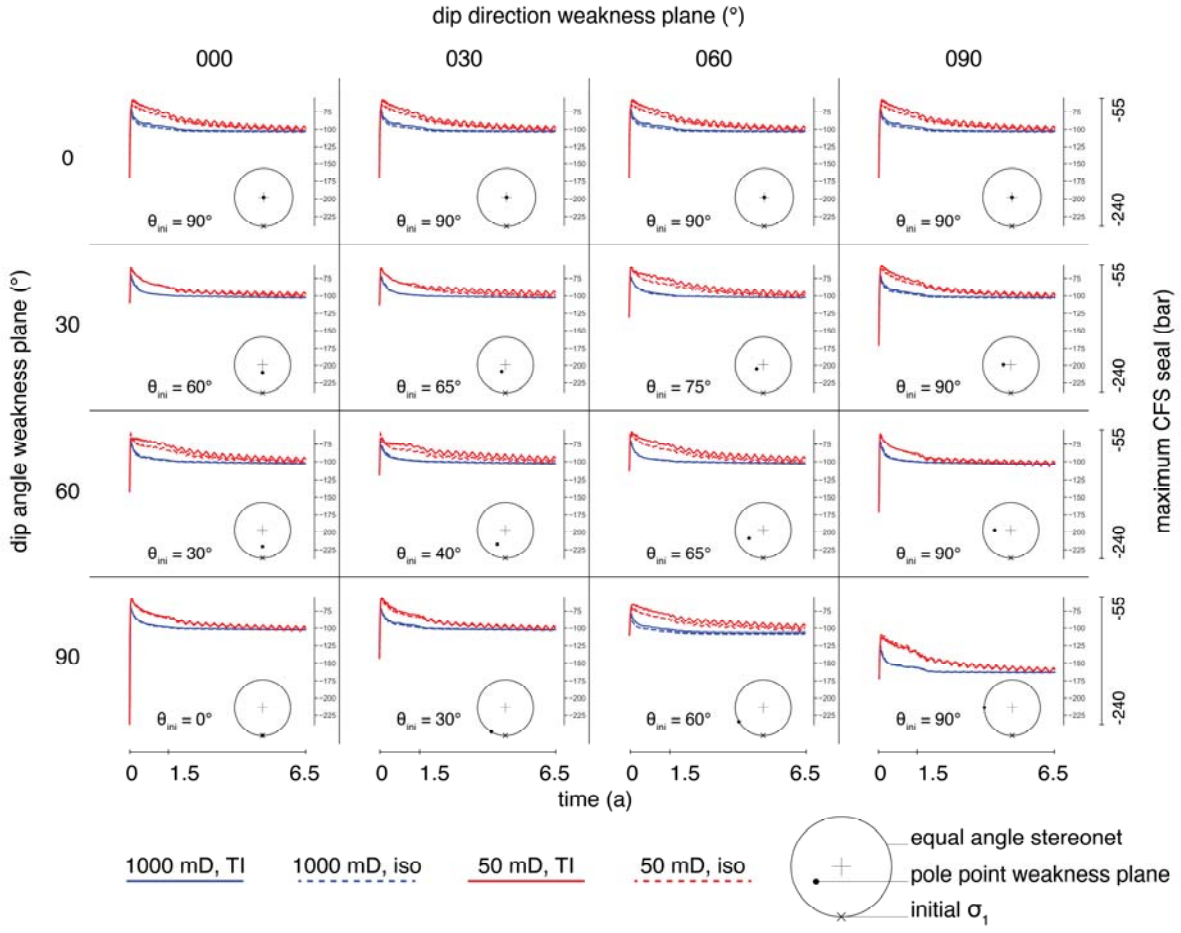


Fig. 3 Comparison of the temporal evolution of the maximum CFS value per timestep in the seal for the different scenarios.

Peak CFS values are similar across all scenarios except the 090/90 scenario and are reached ca. 40 days after start of injection. This indicates that the stability of the seal is governed by the transient thermo-hydro-mechanical stress redistributions and rotations caused by the SH-GES operations. Because the weakness planes are implicitly modelled, they do not affect

the in-situ stresses. The redistributed and rotated stresses are, therefore, identical for a given reservoir permeability and seal anisotropy; different CFS values are, hence, the result of a different weakness plane orientation relative to these transient stresses. The stress redistributions are mostly governed by the far-field stress field, the reservoir permeability, and the elastic anisotropy of the seal. The 090/90 scenario remains comparatively stable throughout, suggesting a mechanically stable orientation of the weakness plane under the given changing stress regime. Fig. 4 highlights how identical stress redistributions (shown as change in differential stress $\sigma_D = \sigma_1 - \sigma_3$; σ_3: minimum principal in-situ stress) lead to different of ΔCFS extents and magnitudes for different weakness plane orientations.

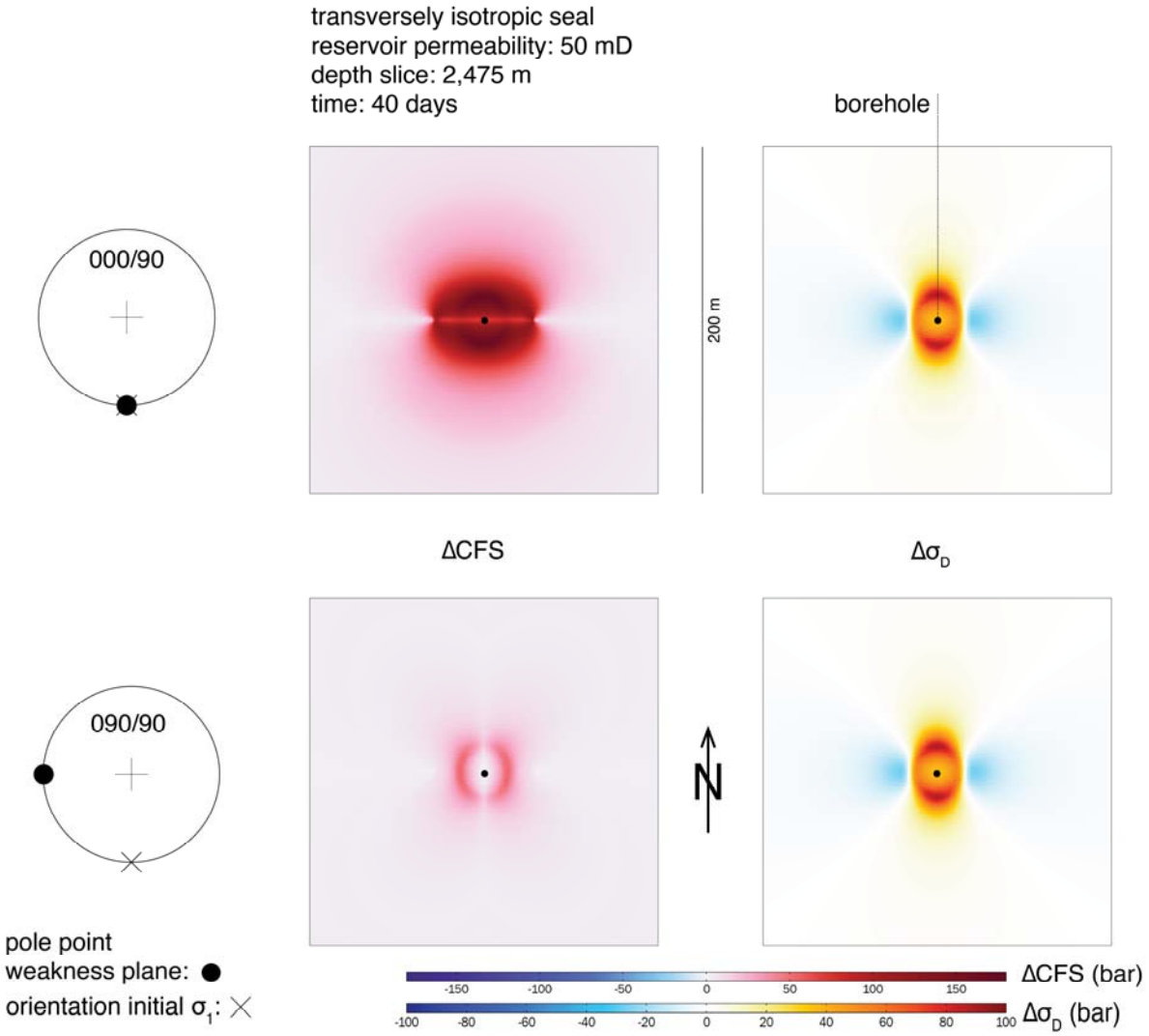


Fig. 4 Comparison of ΔCFS and $\Delta\sigma_D$ for the 000/90 and 090/90 scenarios at the bottom of the seal after 40 days, ± 200 m around the borehole. With τ the shear stress and σ_n the shear and normal stress derived for a given weakness plane orientation, respectively.

A spatial analysis shows that for every weakness plane orientation, the peak CFS value occurs at a different location in a ca. 55 m radius around the borehole. Except for the 090/90 scenario, the peak CFS value as well as the corresponding θ, normal stress σ_n, and shear stress τ values are very similar. For the 090/90 scenario the peak CFS is significantly lower. The corresponding θ is larger than for the remaining scenarios, while σ_n and τ are lower. The quasi-identical peak CFS, σ_n and τ values indicate that a worst orientation of the weakness planes to these altered stresses for which $\theta \approx \theta_{crit}$ can be found for almost every scenario. Only the 090/90 planes are oriented more stable in the given setting.

4 Conclusion

This study examines the impact of elastic and strength anisotropy on the geomechanical stability of a seal formation during Supercharged Hybrid Gas-based Energy Storage (SH-GES). The anisotropy ratio of E/E' = 1.66 leads to only minor differences in seal integrity between isotropic and transversely isotropic models, independent of reservoir permeability. In contrast, seal stability is primarily governed by weakness plane orientation and reservoir permeability. Notably, the initial stability of weakness planes under undisturbed in-situ stress conditions does not predict their time-dependent behaviour during SH-GES operation. Orientations that are initially most stable experience the greatest relative destabilisation over time. This behaviour results from transient stress rotations and stress redistributions induced by coupled thermo-poro-elastic processes. These findings highlight the necessity of time-dependent numerical analyses to accurately assess seal integrity in thermo-mechanical gas-based energy storage systems and other geo-energy applications. The implementation of precise petrophysical parameters, ideally based on upscaling of laboratory measurements, is strongly encouraged.

5 References

This work was supported by a fellowship of the German Academic Exchange Service (DAAD).

Bücken, D., & Backers, T. (2023). *Hybrid CO2 Based Thermo-Mechanical Underground Energy Storage—A Numerical Geomechanical Review*. ISRM-15CONGRESS-2023-468.

Bücken, D., & Backers, T. (2025). *Geomechanical influence of reservoir permeability on supercharged hybrid gas-based energy storage*. KSRM Spring Meeting 2025.

Bücken, D., Backers, T., & Heinze, T. (2026). *Scenario-based sensitivity analysis of petrophysical parameter influence on geomechanical stability during CO2-based thermo-mechanical subsurface energy storage*. SSRN. https://doi.org/10.2139/ssrn.6096839

Buursink, M. L., Anderson, S., Brennan, S. T., Burns, E. R., Freeman, P. A., Gallotti, J., Lohr, C. D., Merrill, M. D., Morrissey, E. A., Plampin, M., & Warwick, P. D. (2023). *Geologic energy storage* (Report Nos 2022–3082; Fact Sheet, p. 4). USGS Publications Warehouse. https://doi.org/10.3133/fs20223082

COMSOL Multiphysics® v. 6.3. www.comsol.com. COMSOL AB, Stockholm, Sweden

Gallo, A. B., Simões-Moreira, J. R., Costa, H. K. M., Santos, M. M., & Moutinho Dos Santos, E. (2016). Energy storage in the energy transition context: A technology review. *Renewable and Sustainable Energy Reviews*, *65*, 800–822. https://doi.org/10.1016/j.rser.2016.07.028

Hudson, J., Harrison, J., & Popescu, M. (2002). Engineering Rock Mechanics: An Introduction to the Principles. *Applied Mechanics Reviews*, *55*(2), B30–B30. https://doi.org/10.1115/1.1451165

Jaeger, J. C. (1960). Shear Failure of Anistropic Rocks. *Geological Magazine*, *97*(1), 65–72. Cambridge Core. https://doi.org/10.1017/S0016756800061100

Li, Y., Yu, H., Xiao, Y., Li, Y., Liu, Y., Luo, X., Tang, D., Zhang, G., & Liu, Y. (2023). Numerical verification on the feasibility of compressed carbon dioxide energy storage in two aquifers. *Renewable Energy*, *207*, 743–764. https://doi.org/10.1016/j.renene.2023.03.013

McLamore, R., & Gray, K. E. (1967). The Mechanical Behavior of Anisotropic Sedimentary Rocks. *Journal of Engineering for Industry*, *89*(1), 62–73. https://doi.org/10.1115/1.3610013

Meier, T. (2017). *Borehole Breakouts in Transversely Isotropic Posidonia Shale*.

Neumann, K. M., Zinke, B., Duda, M., & Backers, T. (2025, March 15). *Experimental investigation of the effect of thermal cycling loading on physical properties of a sandstone from the Upper Rhine Graben*. https://doi.org/10.5194/egusphere-egu25-15455

Paluszny, A., & Zimmerman, R. W. (2025). The role of subsurface geomechanics in the green energy transition. *Royal Society Open Science*, *12*(5). https://doi.org/10.1098/rsos.241516

Wang, W., Yuan, B., Sun, Q., & Wennersten, R. (2022). Application of energy storage in integrated energy systems—A solution to fluctuation and uncertainty of renewable energy. *Journal of Energy Storage*, *52*, 104812. https://doi.org/10.1016/j.est.2022.104812

Winkler, M. B., Frühwirt, T., & Marcher, T. (2023). Elastic Behavior of Transversely Isotropic Cylindrical Rock Samples under Uniaxial Compression Considering Ideal and Frictional Boundary Conditions. *Applied Sciences*, *14*(1), 17. https://doi.org/10.3390/app14010017